NAGW 3624

IN-91-CR

64697   1

P-18

2

ULTRAVIOLET OBSERVATIONS OF THE SATURNIAN NORTH AURORA AND POLAR HAZE DISTRIBUTION WITH THE HST-FOC

J.C. Gérard, V. Dols and D. Grodent

Laboratoire de Physique Atmosphérique et Planétaire,
Institut d'Astrophysique, Université de Liège, B-4000 – Liège, Belgium

J.H. Waite and G.R. Gladstone

Southwest Research Institute, San Antonio, Texas, 78228-0570

R. Prangé*

Institut d'Astrophysique Spatiale, Universit de Paris XI, Orsay, France

February 1995

* Also at Institut d'Astrophysique de Paris

ABSTRACT

Near simultaneous observations of the Saturnian H_2 north ultraviolet aurora and the polar haze were made at 153 nm and 210 nm respectively with the Faint Object Camera on board the Hubble Space Telescope. The auroral observations cover a complete rotation of the planet and, when co-added, reveal the presence of an auroral emission near $80°$ N with a peak brightness of about 150 kR of total H_2 emission. The maximum optical depth of the polar haze layer is found to be located $\sim 5°$ equatorward of the auroral emission zone. The haze particles are presumably formed by hydrocarbon aerosols initiated by H_2^+ auroral production. In this case, the observed haze optical depth requires an efficiency of aerosol formation of about 6 %, indicating that auroral production of hydrocarbon aerosols is a viable source of high-latitude haze.

1. INTRODUCTION

The ultraviolet aurora of Saturn has been studied much less extensively than the Jovian aurora. The first possible detections of the Saturn aurora were ambiguous. The Pioneer 11 ultraviolet photometer observed enhanced emission near the pole possibly due to auroral excitation (Judge et al., 1980). Spatially-resolved spectra were obtained with the International Ultraviolet Explorer (IUE) satellite (Clarke et al., 1980). They showed bursts of H Ly-α which appeared as asymmetries in the north-south distribution of brightness, with variability on a time scale of a few days. The first unambiguous evidence for the Saturnian aurora was provided by the UV spectrometer (UVS) aboard the Voyager 1 spacecraft (Broadfoot et al., 1981; Sandel and Broadfoot, 1981). The UVS measured auroral emission of Ly-α and H_2 Lyman and Werner bands from the polar regions of both hemispheres. Latitudinal slit scans across the south pole located the emission between 78° S and 81.5° S at Saturn System III longitude = 190°, close to the edge of the polar cap determined from the Voyager magnetic field measurements (Ness et al., 1981). In the polar cap, the auroral emission was reduced by at least a factor of 4. The nadir intensity in the oval was estimated $\simeq$ 2.8 kR. Assuming that the magnetic flux through the north and south polar caps are equal, Ben Jaffel et al. (1995) deduced from the detailed UVS observations of the southern aurora that the north aurora lies between 79° N and 82.5° N. North-south scans determined an equatorward boundary of 78° N but the poleward limit of the aurora could not be defined. Further auroral observations were made with the Voyager 2 UVS (Sandel et al., 1981). The average brightness of the north aurora was similar to that measured by Voyager 1. Both observations showed a maximum at 50° $< \lambda_{III} <$180°. They were also consistent with a brightening when the central meridian longitude (CML) is near 50° to 100°. The Voyager 2 data also confirmed that the north emission is confined to a region within 12 degrees of the pole.

In parallel, observations made at 265 nm in the polar regions of giant planets with the photopolarimeter (PPS) aboard Voyager 2 were analyzed by Pryor and Hord (1991). As originally suggested by Lane et al. (1982), they proposed to explain the presence of the dark polar caps as a consequence of the chemical activity generated by the precipitation of energetic particles. In the case of Saturn observations (West et al., 1983), the pressure level probed at 265 nm ranges from 145 mbars at the equator to about 200 mbars at the

pole. The darkening of the polar region is ascribed to the presence of stratospheric haze. The observed northern haze region appears to enclose the auroral zone as defined from the UVS morphological observations. Recently, Ben Jaffel et al. (1995), using the FOC-HST pre-COSTAR images, showed a good correlation between the peak of the haze absorption at 210 nm and the UVS location of the aurora. Pryor and Hord (1991) proposed that H_3^+ ions (produced indirectly by reaction of aurorally-produced H_2^+ with the major atmospheric constituent, H_2) can react with CH_4 to form CH_5^+ which, in turn, can react sequentially with other hydrocarbons to form larger molecules with large absorption cross sections in the ultraviolet. The occurrence of such processes requires that auroral energy is deposited at altitudes with an appreciable methane abundance, i.e., below the methane homopause. This scenario is fully compatible with the nearly coincident location of the haze and the UVS aurora described by Ben Jaffel et al. (1995).

In this study, we report images of the Saturnian north polar region obtained recently with the Faint Object Camera (FOC) aboard the Hubble Space Telescope (HST). A weak signal observed at 160 nm near 80° latitude is interpreted as the signature of the Saturnian auroral emission in the H_2 Lyman bands. A high signal to noise ratio image near 210 nm obtained during the same planetary rotation exhibits a well defined dark polar cap. The latitudinal distribution of the haze darkening is compared with the location of the aurora to investigate the correlation between the ultraviolet emission and the latitudinal polar haze distribution.

2. OBSERVATIONS

The observations were made on October 1 and 2 1994 with the FOC F/96 relay. Since the COSTAR repair has modified the characteristics of the instrument, the new focal ratio of the FOC is F/124. The 1024 × 512 Z zoomed pixel format was used to observe with the largest possible field of view (14 × 14 arcsec). A first exposure was made with the F210 M + F220W filter setup which isolates a 20-nm wide region centered at 210 nm. In addition to avoid excessive count rate leading to non-linearity of the detector's response, the neutral filter F1ND was also used in series with the UV filters. The purpose of this image was both to get a good determination of the UV planetary limb and to analyze the dark haze distribution in the polar cap. A series of 8 1075 sec exposures, each separated

by one HST orbit (96 min) were subsequently made with the F152M + F175W filters in an attempt to image the UV Saturnian aurora over a complete planetary rotation. This filter passband isolates a 20-nm region centered at 153 nm which includes both lines and continuum from the B $^1\Sigma_u$ - X $^1\Sigma_g^+$ Lyman transition. This filter combination was used for previous observations of the Jovian aurora with the FOC and provides good contrast against the sunlight reflected by the planetary disk (Gérard et al., 1993, 1994a,b). Table 1 lists the characteristics of the HST-FOC observations of Saturn. The nominal pointing of the telescope was such that the center of the FOC field of view tracked a point located at a planetographic latitude of 40° N (37° planetocentric) on the central meridian. The same guide stars were used throughout the sequence of observations. It is therefore possible to accurately determine the position of the planet's limb from the image at 210 nm where the planetary disk clearly stands above the sky background. A slight shift of 0.5 arcsec had to be applied to superimpose the NUV image and the nominal limb. During the observations, the phase angle of Saturn was 3.1° and the apparent equatorial and polar diameters were 18.8 and 16.7 arcsec respectively. The planet rotated by 10.5° during each 1075 s exposure.

3. RESULTS

3.1 Auroral morphology

No single image at 153 nm shows a clear auroral contribution. To improve its detectability, all 8 exposures at 153-nm were added together. Figure 1a shows the sum of the 153 nm images rebinned in a 512 × 512 pixel format and smoothed over 5 pixels after sky background subtraction. A portion of the rings and the north polar cap clearly stand up as dark features over the disk. We identify the somewhat brighter zone circling the north pole as the signature of the saturnian UV aurora, although this feature does not strongly contrast with the bright scattered sunlight contribution at lower latitudes.

The characteristics of the auroral morphology are best illustrated in Figure 1b. This figure shows a zoomed and contrast-enhanced version of the average of the 8 images, together with grid of parallels and meridians. The zones of auroral emission are characterized by the density and brightness of pixels defining them. Therefore, a test is applied to each pixel to check the count level and the number of neighboring pixels above a prescribed

level. For comparison, this image overlays the 210 nm image which shows a well defined dark polar region extending down to about 65°N. An alignment of bright features representing the most intense spots of the auroral emission closely follows the 80° parallel and is interpreted as the brightest parts of the UV auroral arc previously detected with the Voyager UVS.

Apparent auroral emission rates may be derived from the count rate in the emission zone using the FOC absolute calibration (including the COSTAR contribution) combined with the filter transmissions. The mean auroral count level above the disk background in the auroral region described before is on the order of 0.2 C pix^{-1}. The total instrument sensitivity in this configuration is $\sim$ 680 MR (megarayleigh) / C pix$^{-1}s^{-1}$ of total H_2 emission (Lyman + Werner bands) . This value is based on a detailed calculation of the FOC response to a synthetic unabsorbed spectrum of the H_2 UV emission excited by 100 eV electrons described in Trafton et al. (1994). Therefore, the average emission level is on the order of 150 kR. This value is larger than the peak values of 40-50 kR detected by the Voyager 1 and 2 UVS observations near $\lambda_{III} = 150°$ which were more typically found to be around 5 kR. It should be stressed, however, that the UVS estimate was based on the assumption that the instrument slit was uniformly filled with auroral emission extending between 78° and 81.5°. The FOC value reported here refers to a more localized region and could therefore be compatible with the UVS observations. The low signal to noise ratio does not permit a detailed study of the longitudinal distribution of the auroral brightness. However, a maximum emission appears to be located in the $\lambda_{III} = 220°$ sector, a region close to that where the UVS observed a maximum brightness. Further interpretation of the longitudinal variation would require further observations.

3.2 Estimate of the total auroral power

The total power radiated by the north aurora may be derived from the integrated count rate of the auroral emission observed at 153 nm. A two-step procedure is applied : (1) the total auroral count rate above the disk background is derived from the data displayed in Figure 1 and (2) the count rate is converted into the total power radiated in the H_2 bands and into a precipitated energy flux. Step 1 first requires a determination of the extent of the auroral emission zone. This determination is based on the contrast enhance-

ment method outlined before. A mask of the emission zone is built and the total number of counts inside it is determined. Using the absolute camera sensitivity and a synthetic H_2 spectrum, we estimate the total H_2 (Werner and Lyman bands) full hemispheric radiated power to be $2.9 \times 10^{10} W$. If an efficiency factor of 7 (Gérard and Singh, 1982; Waite et al. 1983) is used for the conversion of the electron energy flux to the H_2 emission, about 2×10^{11} W must be deposited in the north polar region by the energetic electrons. A precipitated power of $\sim 2 \times 10^{11}$ W was derived from the Voyager 1 UVS observations (Broadfoot et al., 1981) for the two hemispheres. The close agreement between the two sets of observations may be fortuitous, considering the rather poor statistics, possible sources of calibration errors and the high level of variability observed with the Voyager UVS.

3.3 Correlation with the polar haze

As mentioned before, the UV darkening of the polar cap is generally explained by the presence of an additional stratospheric haze layer (West et al., 1983; Karkoschka and Tomasko, 1993). This high altitude layer is possibly generated by the interaction of the auroral energetic precipitation with the Saturnian atmosphere (Lane et al., 1982; Pryor and Hord, 1991; Ben Jaffel et al., 1995). Ben Jaffel et al. (1995) determined that the haze opacity has an equivalent width of $\sim 11°$ centered at $79°$ N. They found that the polar aerosols are very dark (single scattering albedo < 0.07) and is distributed above the 2 mb level.

The present set of data provides a unique opportunity to compare the structures of the auroral UV emission and the UV darkening observed quasi simultaneously. The 210 nm image may be used to map the reflectivity I/F of the Saturnian atmosphere. To characterize the distribution of intensity in the dark north polar region, we consider a radial section from the Sub-Earth point along the central meridian to the north pole, shown in Figure 2a. A slight increase in brightness from the center to about $30°$ is observed near the pole as is apparent from the image in Figure 2a is probably the result of an inadequate flat field correction. To characterize the distribution of the absorption in the north polar region, we assume that the polar haze forms a purely absorbing layer located above the reflecting lower atmosphere as indicated by the results of Ben Jaffel et

al. (1995). In this simple case, the additional absorption by the haze layer is given by $[\exp(-\frac{\tau}{\mu_0})\exp(-\frac{\tau}{\mu})]$, where τ is the polar haze vertical optical depth at 210 nm, μ_0 and μ the local cosines of the solar zenith angle and emission angle, respectively. The procedure adopted is thus to fit the reflectivity distribution of the disk, after removing the polar and ring regions, with a generalized Minnaert function :

$$\ln(\mu I/F) = C_0 + C_1 x + C_2 x^2 + C_3 x^3 \tag{1}$$

where $x = \ln(\mu_0 \mu)$ and C_i denotes constants determined by a least square fit to the observed reflectivity $(I/F)_{obs}$. The synthetic Minnaert distribution $(I/F)_{Min}$ calculated from (1) is then divided by the observed reflectivity $(I/F)_{obs}$ along the central meridian. This ratio is close to unity except in the polar latitudes. The depth of the polar haze is given by :

$$\tau = ln(\frac{I_{Min}}{I_{obs}})(\frac{1}{\mu_0} + \frac{1}{\mu})^{-1} \tag{2}$$

where I_{Min} and I_{obs} are respectively the Minnaert-fitted and the observed distribution directly derived from the 210 nm image.

The latitudinal variation of the optical thickness along the central meridian derived from (2) is shown in figure 2b, together with a least square gaussian fit. Values of τ range from less than 0.1 at latitudes lower than 60° to about 0.27 at 75°. A well defined maximum in τ is located at 75°, about 5° equatorward of the auroral emission.

3.4 Auroral Production of Aerosols

Several sources of high-latitude aerosol production have been suggested by Pryor and Hord (1991) based on the interpretation of the Voyager Photopolarimeter Subsystem. The most plausible appears to be hydrocarbon aerosol formation initiated from aurorally produced H_2^+ ionization. This process is regulated by the production rate of H_2^+ by auroral particle precipitation and the efficiency with which the H_3^+ ions (formed from H_2^+ by rapid ion molecule reaction with H_2, with virtually unitary efficiency in the gas giant atmospheres of the outer planets) react with CH_4 to initiate polymerization. The chemical competition is one between H_3^+ electron recombination and the reaction of H_3^+ with CH_4 to form CH_5^+, a progenitor in the polymerization process. Therefore, the

relative altitude of the methane homopause and the region of maximum auroral electron energy deposition play an important role in determining the efficiency of this auroral aerosol formation process. For example, using the auroral atmosphere described by A-treya et al. (1984) we find that an auroral electron beam of 1 KeV penetrates to an altitude of 110 km near the methane homopause and has an efficiency of approximately 25 % for producing CH_5^+ ions, whereas a 10 KeV electron beam penetrates deeper to 750 km and has almost a 100 % efficiency for producing CH_5^+ ions. Once produced, the CH_5^+ ions can react further with acetylene to form $C_2H_3^+$ or recombine with electrons to form CH_3 or CH_4. The large quantities of atomic hydrogen formed from auroral impact of H_2 will terminate any neutral polymerization schemes through three body recombination reactions of CH_3 and H to reform CH_4. However, ions such as $C_2H_3^+$ can further react with C_2H_2 and continue towards polymerization. We estimate the efficiency of aerosol formation required to produce the observed haze as follows (cf. Pryor and Hord, 1991). Assuming that the haze is made up of spherical particles of radius r and density ρ, the column mass density of haze implied by our derived peak optical depth of $\tau = 0.27$ is given by :

$$N(g\ cm^{-2}) \sim 2 \times 10^{-6}\quad [\frac{\rho}{1}(g\ cm^{-3})]\ [\frac{r}{0.1}(\mu m)] \tag{3}$$

The lifetime of the haze is probably governed by the timescale for gravitational settling through the stratosphere (in the presence of eddy diffusion). A lifetime of ~ 30 years is estimated for such particles from West et al., (1986), so that maintenance of the aerosol layer would require a column mass production rate of

$$P(g\ cm^{-2}s^{-1}) \sim 2 \times 10^{-15}\quad [\frac{\rho}{1}(g\ cm^{-3})]\ [\frac{r}{0.1}(\mu m)] \tag{4}$$

We assume that the aerosol haze is made of 0.1 μm radius particles with a density $\simeq 1$ and extends from the pole to 64 °N, covering about $2.3 \times 10^{19} cm^2$. Thus, we derive an aerosol production rate integrated over the haze cap $\simeq 4.6 \times 10^4$ g s^{-1}. For a typical average brightness of 5 kR (Broadfoot et al., 1981), the H_2^+ column production rate is about 1.7×10^{10} ions cm$^{-2}s^{-1}$. The north aurora emission area, inferred from UVS observations extends from 79^0 to 82.5^0 (Ben Jaffel et al., 1995), covering 2.3×10^{18} cm^2. If we assume that (1) the aerosol composition is dominated by carbon and (2) that all

ions producted below the methane homopause will result in the formation of hydrocarbon ions, we conclude that a typical Saturnian aurora is able to produce the observed haze layer if the aerosol formation (e.g. condensation or clustering on each hydrocarbon ion) is about 6 %.

Based on an aerosol production-loss balance, Pryor and Hord (1991) derived, for a comparable auroral brightness, an efficiency of about 4-25 % and an aerosol production rate of 14-85 $\times$ 10^{-15} g cm^{-2} s^{-1}. Ben Jaffel et al. (1995), using a similar approach, derived a 90 % efficiency and a production rate $\simeq 3 \times 10^{13}$ g cm^{-2} s^{-1}, the discrepancy resulting from a different loss estimate. These production rates should be compared to the 2 $\times$ 10^{-15} g cm^{-2} s^{-1} estimated here.

We note that a 0.1 μm-radius aerosol particle would contain about 2 $\times$ 10^8 carbon atoms, so that the process of going from hydrocarbon ions to aerosols is extremely poorly defined. Our results are merely to demonstrate that auroral production of hydrocarbon aerosols is a viable source for the high-latitude haze.

4. DISCUSSION

A low-level detection of the Saturnian UV aurora has been made with the post-COSTAR HST-FOC. Its local brightness maximum is larger than the values derived from the UVS spectrometer observations aboard Voyager. The observed morphology agrees with the UVS determination of an auroral arc near 80° latitude. The minimum albedo of the dark polar cap, presumably associated with the maximum optical depth ($\simeq 0.3$) of the polar stratospheric haze, is found near 72°-75°, equatorward of the UV auroral peak. Since these two sets of observations were made during a single Saturnian rotation and pointing was using the same guide stars, this conclusion is fairly robust. This result is in good agreement with the conclusions reached by Ben Jaffel et al. (1995) who, using pre-COSTAR HST-FOC images, derived an optical depth of ~ 0.4 near 75° N. The 5°-8° shift between the presumed auroral haze source and the maximum haze absorption may possibly be ascribed to either 1) meridional transport of the precursors of the haze particles by equatorward meridional winds or 2) that the haze latitude represents the average latitude for the aurora, and we have observed a particular aurora at a higher latitude. Since a similar shift on latitude between the haze and the aurora was noticed by Pryor and Hord

(1991), we favor the first possibility. Such winds would be easily generated by the large heat input into the auroral region from precipitating energetic particles. For example, a 100 kR H_2 aurora corresponds to a particle energy flux of about 7 erg $cm^{-2}s^{-1}$ about 50 % of which is converted into gas heating. The latitudinal temperature gradient associated with the auroral heating rate excess over the solar EUV heating will redistribute heat by the combined effect of vertical and horizontal transport in a way similar to the Earth's and probably the Jovian aurora.

Table 1 : main characteristics of the HST-FOC observations of the Saturnian aurora.

Day (1994)	UT	Central wavelength (nm)	CML (λ_{III})	Exposure time (sec)
October 1	22:53	210	77°	1195
October 2	00:30	153	132°	1075
October 2	02:06	153	186°	1075
October 2	03:40	153	239°	1075
October 2	05:16	153	293°	1075
October 2	06:53	153	347°	1075
October 2	08:29	153	42°	1075
October 2	10:06	153	96°	1075
October 2	11:42	153	150°	895

REFERENCES

Ben Jafflel, L. , V. Leers, V. Dols, J.C Gérard and B.R. Sandel, Hubble Space Telescope ultraviolet imaging of Saturn. Evident connection between auroral activity and polar haze, submitted.

Broadfoot, A.L. et al., Extreme ultraviolet observations from Voyager 1 encounter with Saturn, *Science* , **212**, 206, 1981.

Clarke, J.T., H.W. Moos, S.K. Atreya and A.L. Lane, *Nature* , **290**, 226, 1981.

Gérard, J.C, V. Dols, F. Paresce and R. Prangé, Morphology and time variation of the Jovian far ultraviolet imaged with the HST, *J. Geophys. Res.*, **98**, 18793, 1993.

Gérard, J.C., D. Grodent, R. Prangé, J.H. Waite, G.R. Gladstone, V. Dols, F. Paresce, A. Storrs, L. Ben Jaffel and K.A. Franke, A remarkable auroral event on Jupiter observed in ultraviolet with the Hubble Space Telescope, *Science*, **266**, 1675, 1994.

Gérard, J.C and Singh, V., A model of energetic electrons and EUV emission in the Jovian and Saturnian Atmospheres and implications, *J. Geophys. Res.*, **87**, 4525, 1982.

Judge, D.L.,, F.M. Wu and R.W. Carlson, Ultraviolet photometry observations of the Saturnian system, *Science*, **207**, 431, 1980.

Karkoschka, E. and M.G. Tomasko, Saturn's upper atmospheric hazes observed by the Hubble Space Telescope, *Icarus*, **106**, 428, 1993.

Lane, A.L. et al, Photopolarimetry for Voyager 2 : preliminary results on Saturn, Titan, and the rings, *Science*, **215**, 537, 1982.

Ness, N.F., M.H. Acuña, R.P. Lepping, J.E.P. Connerney, K.W. Behannon and F.M. Neubauer, Magnetic field studies by Voyager 1 : preliminary results at Saturn, *Science* , **212**, 211, 1981.

Pryor, W.R. and C.W. Hord, A study of Photopolarimeter system UV absorption data on Jupiter, Saturn, Uranus and Neptune : implications for auroral haze formation, *Icarus*, **91**, 161, 1991.

Sandel, B.R. et al., Extreme ultraviolet observations from the Voyager 2 encounter with Saturn, *Science*, **215**, 548, 1982.

Sandel, B.R. and A.L. Broadfoot, Morphology of Saturn's aurora, *Nature*, **292**, 679, 1981.

Waite, J.H., T.E. Cravens, J. Kozyra, A.F. Nagy, S.K. Atreya and R.H. Chen, Electron precipitation and related aeronomy of the Jovian thermosphere and ionosphere, *J. Geophys. Res.*, **88**, 6143, 1983.

West, R.A., M. Sato, H. Hart, A.L. Lane, C.W. Hord, K.E. Simmons, L.W. Esposito, D.L. Coffeen and R.B. Pomphrey, Photometry and polarimetry of Saturn at 2640 and 7500 Å, *J. Geophys. Res*, **88**, 8679, 1983.

FIGURE CAPTIONS

Figure 1 (a) Log of the sum of the 8 FOC images at 153 nm rebinned over 512 × 512 pixels. The sky background has been subtracted and the data smoothed over 5 × 5 pixels.

(b) Contrast-enhanced zoomed version of (a). A grid of parallels and meridians is superimposed on the synthetic image. Parallels are distant by 10° and meridians are separated by 20° of longitude. The non-auroral image at 210 nm is overlaid to show the location of the auroral emission in comparison with the dark UV polar region.

Figure 2 (a) Center-to-limb variation of Saturn's measured brightness at 210 nm. The dots show the brightness variation measured in a 11-pixel wide cut along the central meridian. The dashed line is the fit of a generalized Minnaert function to the data outside the dark polar cap region.

(b) dots : distribution along the central meridian of the optical depth at 210 nm derived from (a) (see text).

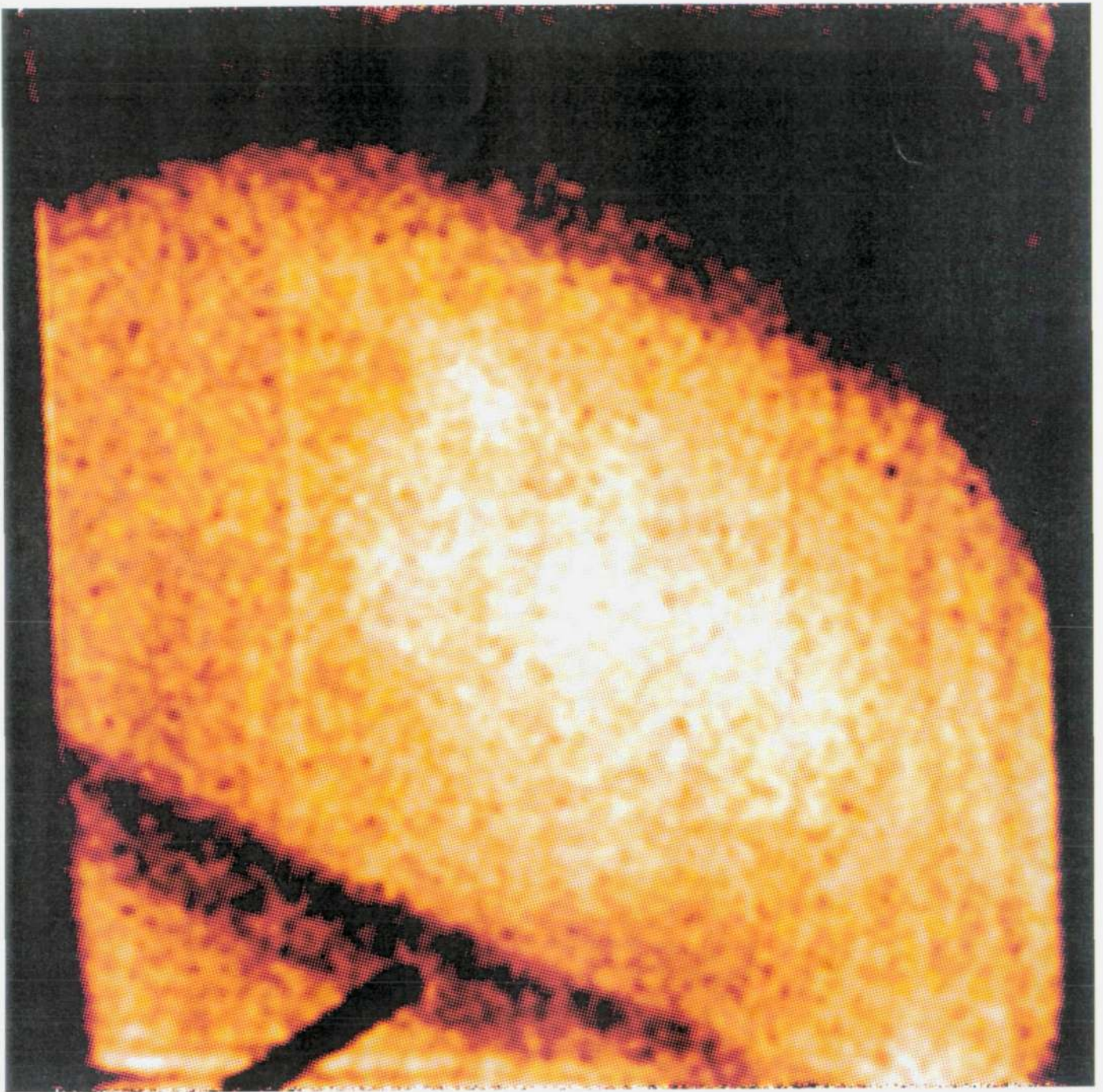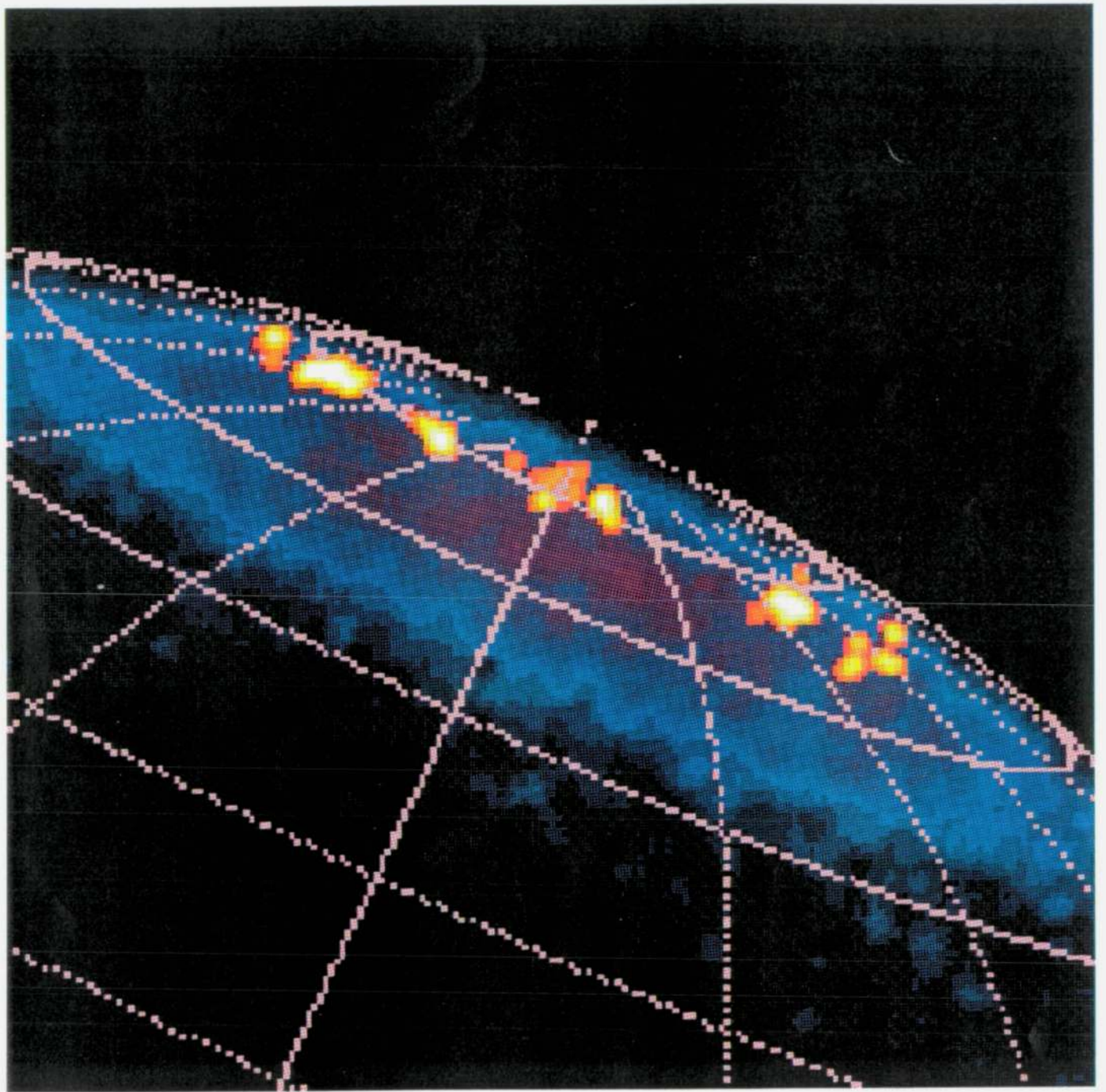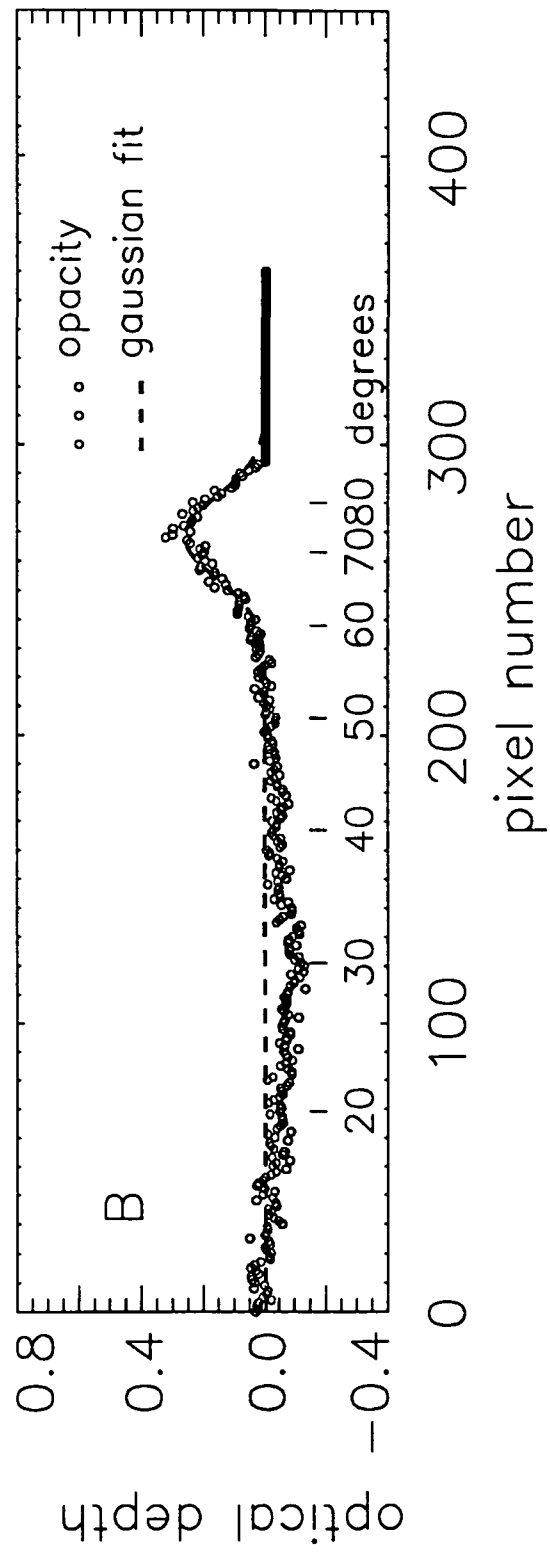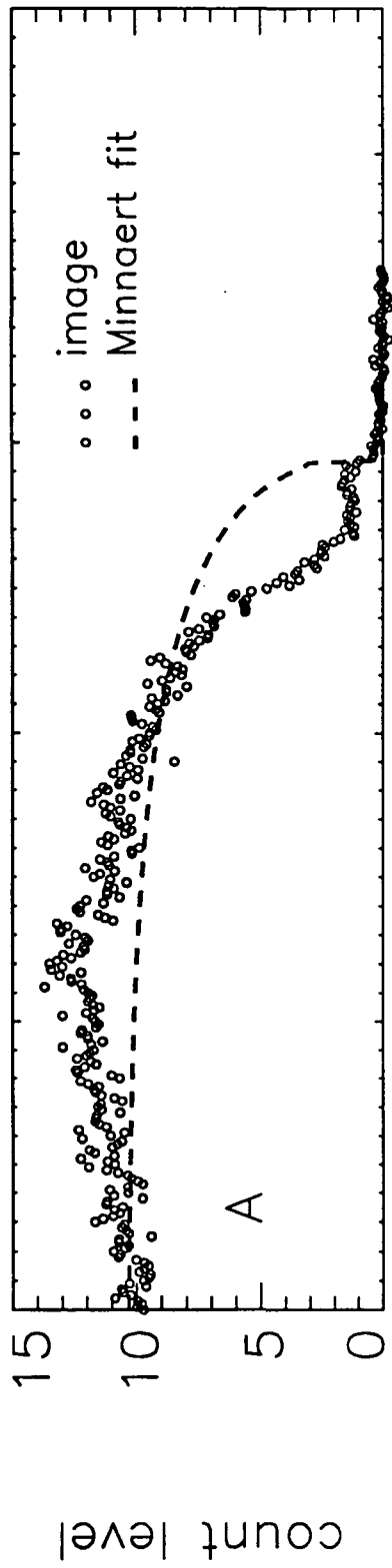dashed line : gaussian fit to the individual data points.

Fig. 1A

Fig. 1B

Fig. 2